First Ground-Based DOAS Measurements of NO_2 at Kinshasa and Comparisons with Satellite Observations

RODRIGUEZ YOMBO PHAKA,[a,b] ALEXIS MERLAUD,[c] GAIA PINARDI,[c] EMMANUEL MAHIEU,[a] FRANÇOIS HENDRICK,[c] MARTINA M. FRIEDRICH,[c] CAROLINE FAYT,[c] MICHEL VAN ROOZENDAEL,[c] BUENIMIO LOMAMI DJIBI,[b] RICHARD BOPILI MBOTIA LEPIBA,[b] EDMOND PHUKU PHUATI,[b] AND JEAN-PIERRE MBUNGU TSUMBU[b]

[a] *Institut d'Astrophysique et de Geophysique, UR SPHERES, Université de Liége, Liége, Belgium*
[b] *Department of Physics, Faculty of Science, University of Kinshasa, Kinshasa, Democratic Republic of Congo*
[c] *Royal Belgian Institute for Space Aeronomy (BIRA-IASB), Brussels, Belgium*

(Manuscript received 28 November 2020, in final form 12 April 2021)

ABSTRACT: We present the first ground-based remote sensing measurements of NO_2 made in Kinshasa. They were performed from 2017 to 2019. The motivation of making observations on air pollution in Kinshasa comes from its geographical location, its demography, its climatic conditions, and the many different sources of NO_2 existing in its surroundings. A method for recovering the vertical density of the NO_2 tropospheric column (VCDtropo) based on the differential optical absorption spectroscopy (DOAS) applied to observations at the zenith and 35° elevation angle is described. The mean value of VCDtropo observed in Kinshasa is 3×10^{15} molecules cm^{-2}. We further present first comparisons with the Ozone Monitoring Instrument (OMI) and Tropospheric Monitoring Instrument (TROPOMI) satellite observations. When comparing OMI data with our observations and using a linear regression analysis, we find a slope of 0.34 and a correlation coefficient of 0.50 for 51 days of coincidences over 2017–19. Similar comparisons with TROPOMI for 44 days show a slope of 0.41 and a correlation coefficient of 0.72. This study opens up perspectives for further air quality–related studies in Kinshasa and central Africa.

KEYWORDS: Instrumentation/sensors; Remote sensing; Satellite observations; Air pollution; Air quality; Atmospheric composition; Measurements; Trace gases

1. Introduction

NO_2 (nitrogen dioxide) is a trace gas that plays an important role in the atmosphere (Crutzen 1979; Brewer et al. 1973). NO_2 is a powerful oxidizing agent, which upon reaction with OH, produces nitric acid, a corrosive substance whose toxic effect destroys the environment (Molina and Molina 2004; Chan et al. 2010). NO_2 is also involved in the formation of tropospheric ozone (Solomon et al. 1999), one of the main components of smog. NO_2 concentrations vary from one region to another, depending on the magnitude of its different sources, such as biomass fires, road traffic, and lightning, and influence of transport. The detection and real-time monitoring of NO_2 is important for the diagnosis of air quality, especially in urban areas. According to the World Health Organization (WHO) guidelines, the yearly annual concentration of NO_2 must not exceed 40 $\mu g\,m^{-3}$ (WHO 2006). Long-term exposure to concentrations above this threshold leads to respiratory and cardiovascular diseases.

Recent studies show that Africa is being overtaken by the problem of air pollution (Knippertz et al. 2015). According to a study published by the Organization for Economic Cooperation and Development (Roy 2016), the number of premature deaths related to air pollution in Africa increased by 36% between 1990 and 2013. Research also shows that air quality in urban areas in Africa, defined in particular by black carbon, organic carbon, CO, NO_x (NO and NO_2), SO_2, and nonmethane hydrocarbon concentrations, is expected to deteriorate rapidly in the coming decade, with concentrations of NO_2, aerosols, and other combustion products anticipated to be on the rise (Liousse et al. 2014).

Kinshasa (4.32°S, 15.18°E) is the capital of the Democratic Republic of the Congo (DRC) and the third most populated city in Africa (12 million) and it could reach 30 million inhabitants by 2030 (UN 2016). Up to very recently, there were no continuous measurements of air pollution performed from the ground in this city (Katoto et al. 2019) and the few observations in terms of NO_2 pollution available are those measured by satellite instruments.

Figure 1 shows the different seasonal situations of NO_2 tropospheric pollution around DRC from 2018 to 2019, as seen by the TROPOMI instrument. A seasonal cycle of NO_2 pollution can be observed in this area, with a pollution spot always present and visible from the satellite during the whole period of the year in Kinshasa. Although not visible on the various frames of Fig. 1 given the size of the selected area, Kinshasa most of the time shows a vertical column density (VCD) in the upper range of the scale, i.e., above 2×10^{15} molecules cm^{-2}. The highest values of NO_2 for the whole observation area are observed between the months of June and August, corresponding to the dry season.

During the dry seasons, the peasant population living around Kinshasa and in almost all provinces of the DRC burns the savannah and forest in order to prepare the land for cultivation, producing pollutant emissions in atmosphere. In addition to those emissions, there are emissions of polluting

Corresponding author: Rodriguez Yombo Phaka, rodriguez2yombo@gmail.com

DOI: 10.1175/JTECH-D-20-0195.1

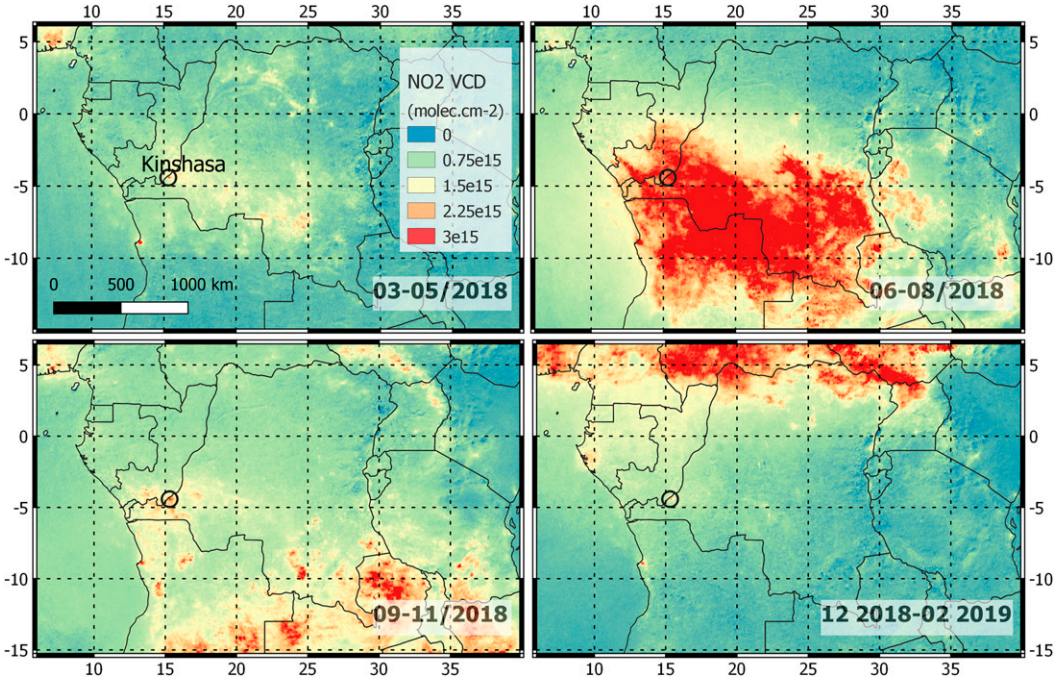

FIG. 1. Maps of mean tropospheric NO_2 VCDs [from Royal Netherlands Meteorological Institute (KNMI)/European Space Agency (ESA) data processed at BIRA-IASB derived from TROPOMI observations over central Africa during the year 2018].

species by industrial entities poorly equipped with fume washing systems, by diesel generators that compensate for the inadequacies of electricity distribution, by the combustion of waste piled up in open dumps, and also by road traffic, which is mainly old vehicles. The management and mitigation of a problem such as air pollution requires a good knowledge of the phenomenon, which varies from one region to a another. Understanding the specific situation of Kinshasa first requires the collection of data to carry out studies, which are then used in support of the prevention and management of episodes of pollution peaks, further aimed at informing in quasi–real time the population about the pollution levels.

To address the critical lack of data in this region, the Royal Belgian Institute for Space Aeronomy (BIRA-IASB) and the University of Kinshasa (UniKin) have set up a collaboration that led to the installation of an atmospheric remote sensing instrument in May 2017 on the UniKin site. This instrument, based on the differential optical absorption spectroscopy (DOAS) technique, is capable of continuous unattended operation.

DOAS instruments have been widely used for measuring NO_2 in the troposphere as well as in the stratosphere (Platt and Stutz 2008). First used for stratospheric NO_2 measurements using scattered light observations at zenith (Noxon 1975), more recent efforts have focused on tropospheric NO_2 in urban environments (e.g., Kramer et al. 2008; Gielen et al. 2017; Chen et al. 2009; Zhao et al. 2020; Ialongo et al. 2020; Friedrich et al. 2019).

This work presents NO_2 tropospheric vertical column densities retrieved from measurements made in Kinshasa between May 2017 and November 2019. It also compares the ground-based observations with NO_2 measurements made by two satellite instruments [Ozone Monitoring Instrument (OMI) and Tropospheric Monitoring Instrument (TROPOMI)]. This manuscript is organized as follows: Section 2 provides a description of the observation site, the instrument, and the method used to analyze the measurements. Section 3 describes the algorithm used to obtain the tropospheric vertical columns of NO_2 and the approach for filtering out erroneous data. The interpretation and the discussion of the results are presented in section 4, with emphasis on comparisons between the ground-based and satellite measurements.

2. Site, instrument, and spectral analysis

a. *Observation site*

The city of Kinshasa extends over an area of 9965 km^2 along the southern bank of the Pool Malebo and constitutes a flat low surface at an average altitude of about 300 m MSL (Saint-Moulin 2011). Situated between latitudes 4.30° and 4.50°S and between longitudes 15.14° and 15.32°E, the city of Kinshasa is bounded to the west and north by the Congo River, forming the natural border with the Republic of the Congo Brazzaville (see Fig. 2). Our observations were made at the UniKin (4.41°S, 15.31°E), 13 km from the river and south of the city as indicated by the red dot in Fig. 2. Kinshasa lies in a hot and humid tropical climate, with an average annual temperature of 25°C and an average annual rainfall of 1,400 mm. It rains in Kinshasa on average 112 days a year with a peak of 18 rainy days in April (Shomba Kinyamba et al. 2015). The city has two seasons: a rainy season and a dry season. The rainy period extends from

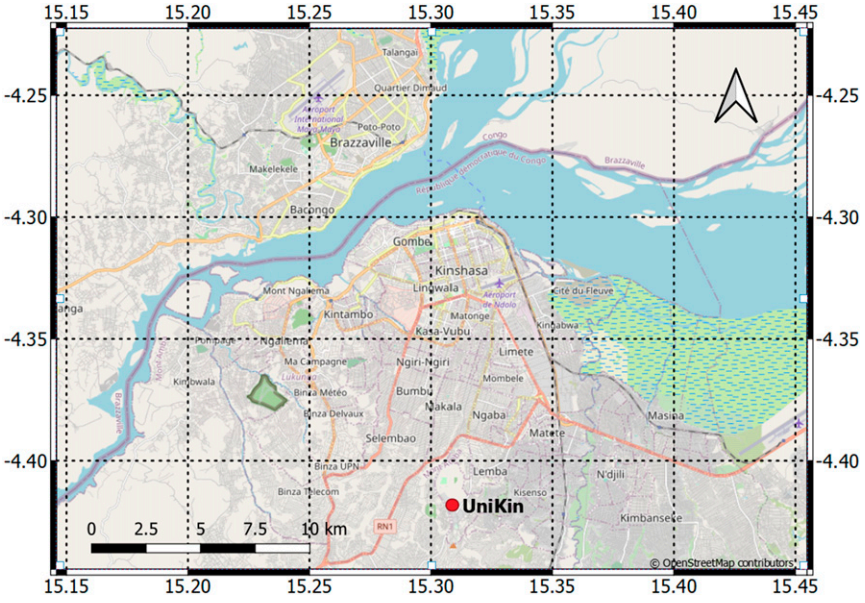

FIG. 2. Map of Kinshasa with position of the UniKin site.

mid-September to mid-May, with peaks of heavy rainfall in November and April. The dry season covers the period from mid-May to mid-September. The atmosphere of the city of Kinshasa is strongly influenced by clouds and aerosols, the abundance of which varies with the seasons.

Figure 3 shows the time series of aerosol optical depth (AOD) in the vicinity of Kinshasa as observed by the Moderate Resolution Imaging Spectroradiometer (MODIS) instrument at 550 nm and converted to 477 nm using the Angstrom relationship. It shows that the values range from 0.1 to 1.5, with extreme values up to 2.5 (data from https://giovanni.gsfc.nasa.gov/giovanni/). These observations indicate a cyclical presence of aerosols around Kinshasa, mainly due to forest fires as mentioned in the introduction. It can also be seen that the periods when maximum AOD values are observed correspond exactly to the periods when maximum NO_2 values are also observed by the satellite as seen in Fig. 1.

b. *Instrumental setup*

The instrument used in this work is based on an Avantes ULS2048-XL spectrometer, covering the spectral range 280–550 nm at a spectral resolution of 0.7 nm full width at half maximum (FWHM). The spectrometer is a Czerny–Turner type with a focal length of 75 mm, an input slit of 50 μm width, and a 1200 L mm^{-1} grating. An optical fiber of diameter 600 μm is connected to the UV–VIS spectrometer. The spectrometer is directly connected to a computer that controls the acquisition and record the spectra. We record after each minute of observations a spectrum representing intensity as a function of wavelength. From May 2017 to November 2017, measurements were carried out in the zenith sky geometry, pointing the telescope toward the zenith at a 90° elevation angle. From July 2018 to November 2019, the instrument measured toward a 35° elevation angle and a 58° azimuth (NE). The gap in the observation period is caused by technical difficulties with the instrument, the change of observation strategy had to be implemented due to security issues. In addition to fixed geometry measurements, we also used an amateur telescope (Celestron Nexstar) (Yombo et al. 2018) to perform experimental measurements in multiaxis mode (Hönninger et al. 2004). Table 1 lists the different observation situations for each period.

c. *DOAS analysis*

The QDOAS software (Danckaert et al. 2017) developed at BIRA-IASB is used to obtain differential slant-column densities (DSCDs), which represent the difference between the slant-column densities (SCDs; the integrated trace gas concentrations along the light path) of the measured and the reference spectra.

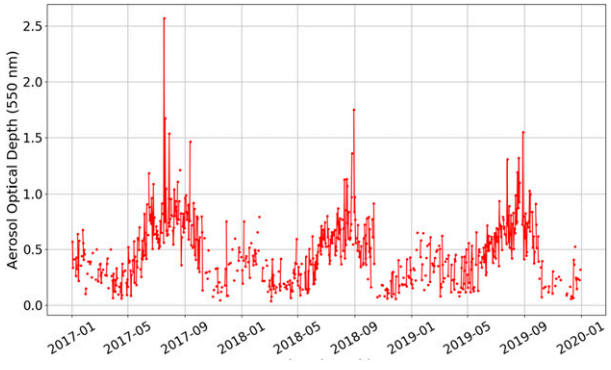

FIG. 3. Time series of the monthly aerosol optical depth (AOD) observed at 550 nm wavelength by the MODIS *Terra* instrument downloaded from https://giovanni.gsfc.nasa.gov/giovanni/ for an area covering the city of Kinshasa (3–5°S, 14–16°E).

TABLE 1. Observations setup: Measurements at the zenith were interrupted due to insecurity at the observation site. Thus, we were pushed to change the location of observation, which only offered the possibility to make the measurements at 35° elevation angle. Measurements in MAX-DOAS were made only for a few days because of the difficulties en countered in the field. The lack of electricity meant that measurements could not be taken every day.

Observation period	Settings
May–Nov 2017	Zenith measurements
2 Oct 2017	MAX-DOAS measurements with an amateur telescope (Nexstar)
Dec 2017–Jun 2018	No ground-based observations due to fiber breakage
Jul 2018–Mar 2019	Measurements at 35° elevation and 58° NE azimuth
Mar–Nov 2019	Measurements removed from the database because of dust accumulation
Nov 2019	Measurements resumed at 35° elevation and 58° NE azimuth

The DOAS fit was performed in a small wavelength window in which the concerned absorber, in our case NO_2, shows strong and prominent absorption features. NO_2 has its strongest absorption lines in the 425–490 nm region. Here, other species such as O_3, H_2O, and O_4 also show strong absorption, which need to be included in the QDOAS analysis. The contributions of Rayleigh and Mie scattering that vary slowly with wavelength are removed by introducing a polynomial of degree 5. In addition to the elastic (Rayleigh, Mie) contributions, we added a synthetic ring spectrum to correct for the ''filling-in'' effect on Fraunhofer lines, known as the ring effect, which originates from the Raman rotational scattering of oxygen and nitrogen molecules (Chance and Spurr 1997). QDOAS settings and cross sections adopted for the analysis are listed in Table 2.

Figure 4 shows a typical DOAS result for NO_2. The analyzed spectrum is of 1417 UTC 11 August 2017 (SZA = 51.62°) and the reference spectrum comes from the multiaxis DOAS (MAX-DOAS) observations on 2 October 2017. The first four panels show the absorptions of NO_2 (Fig. 4a), water vapor (Fig. 4b), ozone (Fig. 4c), and the collision complex O_2–O_2 called O_4 (Fig. 4d) as optical densities relative to the reference spectrum. The last panel displays the fit residuals. Black lines correspond to molecular cross sections scaled to the detected absorptions in the measured spectrum. The calculated contributions refers to the NO_2 cross section (as function of wavelength) multiplied by the retrieved NO_2 DSCD; the latter is also given in Fig. 4a and is $(1.46 \pm 0.057) \times 10^{16}$ molecules cm^{-2}.

3. NO_2 vertical column retrievals

The method used to convert DSCDs to tropospheric vertical column densities (VCD_{tropo}) is an adaptation of the ones explained by Tack et al. (2015), Constantin et al. (2013), and Chen et al. (2009). The conversion from a total SCD to a total vertical column density is performed using the airmass factor (AMF) as shown in Eq. (1):

TABLE 2. Main DOAS analytical parameters for the retrieval of NO_2 DSCD, closely related to the NDACC UV–VIS Working Group standard recommendations (Van Roozendael and Hendrick 2012).

Parameters	Settings
Fitting interval	425–490 nm
Calibration	Chance and Kurucz (2010)
NO_2	Vandaele et al. (1998), 298 K
O_3	Bogumil et al. (2003), 223 K
H_2O	Harder and Brault (1997)
O_4	Hermans et al. (2003)
Correction ring effect	Chance and Spurr (1997)
Polynomial term	Polynomial of order 5
Offset intensity correction	Offset (constant), offset (order1); nonlinear

$$\mathrm{VCD} = \frac{\mathrm{SCD}}{\mathrm{AMF}}. \tag{1}$$

VCD represents a geophysical quantity that can be used for comparison with other measurements, such as those from satellites. AMF represents the proportionality factor between the slant column density and the vertical column density. It depends on the parameters influencing the transfer of the solar radiation through the atmosphere, i.e., pressure, temperature, aerosols, clouds, surface albedo, vertical profiles of important absorbers, and the profile of the measured absorber (Hönninger et al. 2004). We have calculated the AMFs used in this work with a radiative transfer model (RTM) as described in section 3c. The SCD can be obtained from retrieved DSCDs by adding the NO_2 contribution of the reference spectrum ($SCD_{residual}$), used in the fit of the retrieved DSCDs, according to

$$\mathrm{SCD} = \mathrm{DSCD} + \mathrm{SCD}_{\mathrm{residual}}. \tag{2}$$

To determine the tropospheric slant-column density (SCD_{tropo}), the stratospheric slant-column density (SCD_{strato}) is subtracted from the SCD:

$$\mathrm{SCD}_{\mathrm{tropo}} = \mathrm{SCD} - \mathrm{SCD}_{\mathrm{strato}}. \tag{3}$$

In light of Eq. (1), we calculate the VCD_{tropo} directly, dividing the SCD_{tropo} by the tropospheric airmass factors (AMF_{tropo}):

$$\mathrm{VCD}_{\mathrm{tropo}} = \frac{\mathrm{DSCD} - \mathrm{SCD}_{\mathrm{strato}} + \mathrm{SCD}_{\mathrm{residual}}}{\mathrm{AMF}_{\mathrm{tropo}}}. \tag{4}$$

The determination of the unknown components ($SCD_{residual}$, SCD_{strato}, AMF_{tropo}) is discussed in the following subsections.

a. Determination of the stratospheric column density

The stratospheric NO_2 column can be retrieved during the twilight period, when the photon light path becomes larger in the stratosphere than in the troposphere (e.g., Van Roozendael and Hendrick 2012). In our case, however, due to the low sensitivity of the instrument, our measurements do not reach solar zenith angle (SZA) near 90° (Fig. 5, blue dots). Therefore, we calculated the NO_2 SCD_{strato} using the model UVspec/DISORT

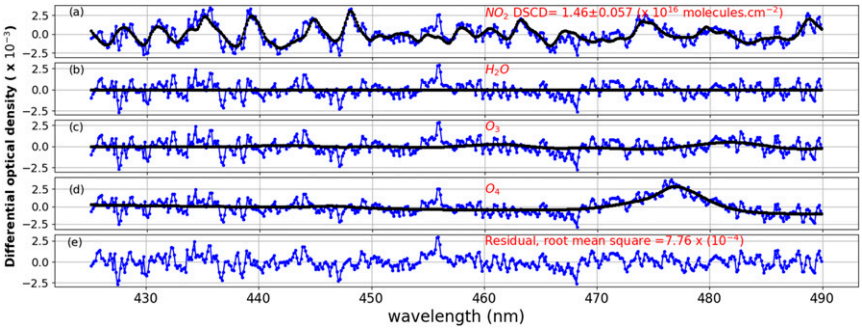

FIG. 4. Example of a DOAS fit of a spectrum recorded at 1417 UTC 11 Aug 2017 (SZA = 51.62°). Black lines correspond to molecular cross sections scaled to the detected absorptions in the measured spectrum (blue lines).

RTM (Mayer and Kylling 2005) coupled with the photochemical box model PSCBOX (Errera and Fonteyn 2001; see also Hendrick et al. 2004; Tack et al. 2015).

Simulations of SCD_{strato} were done for the first and the fifteenth of each month of our study period. Figure 5 (black dots) shows an example of the modeled stratospheric slant columns for 15 August 2018. The figure also shows the measured DSCDs for these days (blue dots). The daily behavior of these columns is explained by the geometry of the measurements. This "U" behavior is related to the optical path in the atmosphere which increases at sunrise and sunset. The effect is particularly visible for NO_2 because this molecule is also present in the stratosphere where the geometrical enhancement is very important when the sun reaches (and exceeds) the horizon.

In practice, we interpolate in this modeled SCD^{model}_{strato} lookup table for the days of interest and normalize by the measured OMI NO_2 stratospheric VCD (VCD^{OMI}_{strato}) using the following equation:

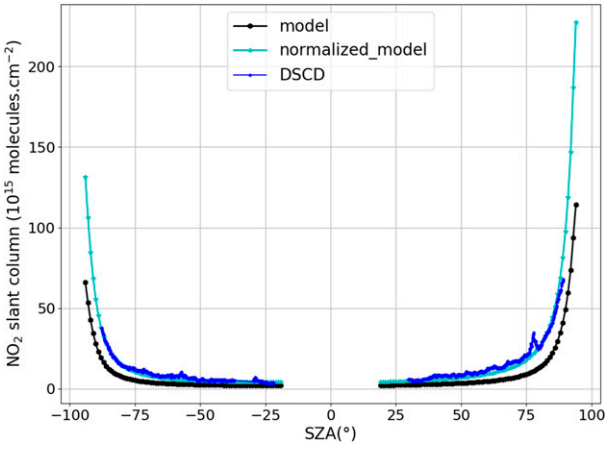

FIG. 5. Example of the stratospheric column density calculated using the UVspec/DISORT RTM coupled with a photochemical box model PSCBOX for 15 Aug 2018 (black dots). Illustration of the DSCDs measurements on 15 Aug 2018 (blue), and an example of the standardization of the model's SCD_{strato} by OMI observations (cyan dots). The negative values of SZA correspond to the morning and the positive values are during the evening.

$$SCD^{norm}_{strato} = VCD^{OMI}_{strato} \times \frac{SCD^{model}_{strato}}{VCD^{model}_{strato}}, \quad (5)$$

where VCD^{model}_{strato} is the modeled stratospheric NO_2 at the OMI overpass time.

Finally, as we retrieve the NO_2 absorption in our spectra with a cross section recorded at 298 K, this cross section is underestimated for the stratospheric NO_2. This leads to an enhancement of the stratospheric NO_2 signal in our measured DSCDs. We correct this by multiplying the modeled stratospheric NO_2 by 1.2, a factor corresponding to the factor between the NO_2 DSCDs retrieved at 220 K (typical temperature of the stratosphere) and 298 K (Vandaele et al. 1998).

Figure 5 (cyan dots) illustrates SCD^{norm}_{strato} obtained for 15 August 2018.

b. *Determination of the residual NO_2 column in the reference spectrum*

The DOAS analysis requires the use of a reference spectrum. Ideally, this reference spectrum would represent the light of the sun before entering in Earth's atmosphere. However, with ground-based measurements like ours, this is not possible. The reference spectrum thus contains a residual absorption that must be quantified independently of the DOAS analysis.

In our case, we used a reference spectrum recorded with a low-cost MAX-DOAS system, under clear-sky conditions from 1202 UTC 2 October 2017 at zenith. Since we also measured spectra at 30° during this MAX-DOAS acquisition, we can retrieve the reference tropospheric column under a geometric approximation (Hönninger et al. 2004). We estimated the stratospheric contribution to the reference column from the model simulations explained in section 3a. The total value of this residual column is estimated to be 0.65×10^{16} molecules cm^{-2}, as the sum of the tropospheric contribution (0.5×10^{16} molecules cm^{-2} obtained from MAX-DOAS measurements) and the stratospheric contribution (0.15×10^{16} molecules cm^{-2} obtained from model simulations). To analyze observations made at 35°, we changed the reference spectrum to a 35° spectrum from 1202 UTC 14 August 2018. The residual column was adapted by adding the offset of 0.3×10^{16} molecules cm^{-2} coming from the difference between DOAS analyses made with the two reference spectra. Note that we changed the

reference spectrum to reduce the effect of spectrometer instabilities and improve the DOAS analysis.

c. *Tropospheric airmass factor*

Tropospheric AMF calculations were performed using the Vector Linearized Discrete Ordinate Radiative Transfer model (VLIDORT) (Spurr 2013). As mentioned above, the AMF calculation is intrinsically dependent on the site's observation conditions and the profile of the concerned absorber. Thus it is interesting to perform several tests to arrive at realistic parameters for the calculation of this AMF. The NO_2 profiles were retrieved from a GEOS-Chem 3D Chemistry Transport Model full chemistry simulation, using version 12.0.2 driven by MERRA-2 meteorological fields (Bey et al. 2001; see also http://wiki.seas.harvard.edu/geos-chem/index.php/GEOS-Chem 12). Our simulation covers the period from 2017 to 2019. The temperature and pressure profiles used in VLIDORT come from global meteorological reanalysis of the European Centre for Medium-Range Weather Forecasts (ECMWF) taken over the 20-yr period. VLIDORT takes the total-layer extinction and total-layer single-scattering albedo as well as total-layer phase function moments and returns the intensity (among other things that can be configured). The total-layer input parameters are calculated from the contributions of the gas, air, and aerosols. For this, we choose a trace-gas concentration (for trace-gas absorption), air density and wavelength (for Rayleigh scattering contribution), and aerosol properties such as single-scattering albedo and asymmetry parameter with the Henyey–Greenstein phase function to calculate the aerosol phase function moments. The geophysical parameters used in the VLIDORT simulations are described in Table 3.

Figure 6 shows selected monthly averages of the NO_2 profile extracted from the GEOS-Chem simulation (2018) and a simple box model corresponding to a highly concentrated NO_2 200-m-thick layer above the surface. The box profile helped us to evaluate the error in the calculation of the tropospheric AMF as explained in section 4b. In Fig. 6, GEOS-Chem profiles show that in the lower troposphere (between the surface and 3 km) the highest NO_2 values are obtained for the months of June to September. This period corresponds to the dry season, when forest fires are often observed around Kinshasa (see Fig. 3).

The boundary layer height (BLH) above Kinshasa exhibits daily variations with a sharp increase at 0600 UT, a maximum every day at 1200 UT and a sharp decrease from 1500 UT. The minimum BLH happens in June (900 m at 1200 UT), while the maximum is reached in September (1300 m) [Copernicus Climate Change Service (C3S); C3S 2017].

When performing sensitivity tests, we find that the calculated AMFs vary strongly with the SZA, the AOD, and the NO_2 profile. On the other hand, they depend weakly on the change in temperature (T) and pressure (P) profiles. On this basis, we use constant T and P profiles in VLIDORT. The box profile has a considerable influence on the calculated AMF; that is why we use it in section 4b to estimate the error in this AMF calculation. The sensitivity test also showed that AMFs calculated under Kinshasa conditions are less dependent on the change in GEOS-Chem profile during the year. We have therefore set a unique GEOS-Chem profile in VLIDORT. Figure 7 illustrates the sensitivity tests performed on AMFs (90° and 35°) as a function of SZA and for different AODs. We obtain realistic AMFs for Kinshasa conditions by interpolation through the tropospheric NO_2 AMF lookup table created at AOD values measured by the MODIS instrument.

4. Results and discussion

In this section, we present the retrieved tropospheric NO_2 VCDs. Data recorded under dark or heavy cloud conditions are filtered out from the analysis. An uncertainty budget is described and we finally present a comparative study between our retrieved NO_2 VCDs and observations made by two satellite instruments (OMI and TROPOMI).

a. *NO_2 tropospheric vertical column*

Figure 8 illustrates our NO_2 VCDtropo retrievals. Figures 8a and 8b show the VCDtropo for 24 August and 11 October 2017 with the corresponding DSCDs. The DSCDs follow a "U" shape related to the optical path during the day. The AMF corrects this "U" shape for the VCDtropo, which range for these two days between 1×10^{15} and 12×10^{15} molecules cm^{-2}. Figures 8c and 8d show the VCDtropo for August and October 2017, which are during the dry season and the wet season, respectively. Blue dots indicate the individual VCDtropo retrievals while the red lines are the daily averages. Although we retrieve the highest individual VCDtropo in early October, the daily averages are generally lower in October than in August.

b. *Error estimation*

The main sources of uncertainty in VCDs are related to each component used in Eq. (4). The uncertainty on the tropospheric VCD (σ_{VCD}) can be calculated as follows:

$$\sigma_{VCD}^2 = \left(\frac{\sigma_{DSCD}}{AMF_{tropo}}\right)^2 + \left(\frac{\sigma_{SCDstrato}}{AMF_{tropo}}\right)^2 + \left(\frac{\sigma_{SCDresiduel}}{AMF_{tropo}}\right)^2 + \left(\frac{SCD_{tropo}\sigma_{AMF_{tropo}}}{AMF_{tropo}^2}\right)^2. \quad (6)$$

In Eq. (6), each error contribution has a different source, independent of the other terms. Therefore, there is no correlation between these different sources. The four contributions of Eq. (6) are, respectively, as follows:

1) The error on the DOAS fitting (σ_{DSCD}). This error has two contributions, the random error (caused by noise in spectral measurements) and a systematic error, related to the error on the effective cross section of the NO_2. We estimated a random error to be 0.5×10^{15} molecules cm^{-2} by taking the mean of all the error values of the slant columns of NO_2 as analyzed with QDOAS. The systematic error was estimated at 3% in accordance with the study made by Vandaele et al. (1998).
2) The error on the stratospheric SCD ($\sigma_{SCDstrato}$) is the uncertainty on the stratospheric slant column simulated by the RTM UVspec/DISORT coupled to the photochemical

TABLE 3. Geophysical parameters for the calculation of VLIDORT inputs to perform the radiative transfer simulations used in the tropospheric AMFs calculation. The sensitivity test showed that the calculated AMFs are predominantly influenced by the NO_2 profile and the AODs. The NO_2 profiles were extracted from a full-chemistry GEOS-Chem version 12.0.2 simulation covering the period from 2017 to 2019. The different AOD values were taken in relation to the cycle of cloud variability in different seasons in Kinshasa.

Parameters	Settings
Surface albedo	0.06
Wavelength	477 nm
Pressure and temperature profile	Standard atmosphere
A priori profile	Linearly decreasing profile from 0.3 ppb at 0 km to 0.01 ppb at 4 km
Aerosol profile	Box profile from the surface to 550 m above ground
Aerosol extinction	0.0, 0.1, 0.3, 0.5, 1, offset
Asymmetry parameter	0.68

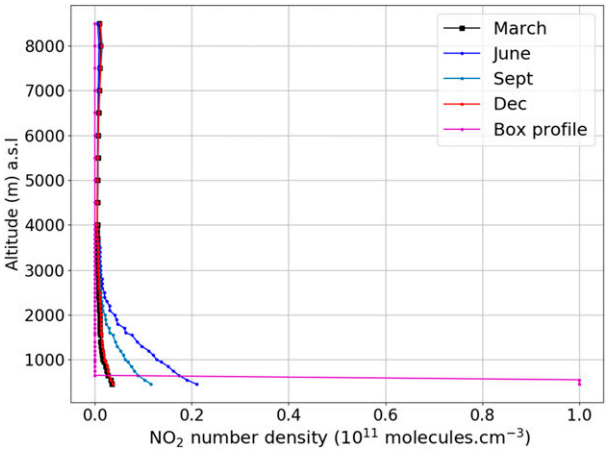

FIG. 6. Mean monthly profiles of NO_2 extracted from the GEOS-Chem simulation during the year 2018 and a box profile. Note that the surface is 400 m above sea level.

model PSCBOX. This error source is discussed in Tack et al. (2015) and references therein. Conservative estimates of the errors on the photochemical and RT components of the stratospheric NO_2 SCD simulation reach 20% and 10%, respectively. By adding both error components in quadrature, this leads to a total error of 22% on the SCD model (or 0.5×10^{15} molecules cm^{-2} based on the simulated NO_2 SCD_{strato} mean value around OMI overpass time over Kinshasa).

3) The error on the residual amount of NO_2 in the reference spectra $SCD_{residual}$. We estimated the residual slant column error by propagating the error across all components used to estimate the residual column. This error has been estimated at 1.3×10^{15} molecules cm^{-2} for zenith measurements and 1.8×10^{15} molecules cm^{-2} for 35° measurements, as 20% of the $SCD_{residual}$ value used for the measurements in each case.
4) Errors in the calculation of the tropospheric AMF are related to uncertainties in the input parameters used in the VLIDORT RTM. In Chen et al. (2009), an extensive sensitivity test was performed considering various input parameters in radiative transfer simulations. The influence of parameters such as aerosol and NO_2 layer height, AOD and NO_2 profile, and surface albedo was tested. Based on this sensitivity analysis, the uncertainty on the AMF was estimated to be in the range of 10%–20% for SZA between 20° and 85°. By considering the difference between AMFs calculated with profiles extracted from GEOS-Chem and those calculated with a simple box profile, we estimated the uncertainty on the tropospheric AMF used in this study to be about 0.35 for the AMF calculated at 90° and 0.15 for those calculated at 35° (mean values taken at overpass). The use of a box profile is justified by the fact that in polluted regions, the bulk of the NO_2 concentration is generally close to the surface.

The error budget presented in Table 4 indicates that the main source of error is tropospheric AMF. Calculations show that, for all measurements, the median of uncertainty on the tropospheric NO_2 VCD is 25% for zenith measurements and 23% for 35° measurements.

c. *Comparison with satellite observations*

The OMI is a nadir imaging spectrometer operating in two spectral bands (UV: 270–380 nm; visible: 350–500 nm) on board the *Aura* satellite (Levelt et al. 2006). The size of its ground pixels varies from 13 km × 24 km at nadir to 28 km × 150 km at the swath edges. We show comparisons between our ground-based measurements and the OMI QA4ECV NO_2 product (Boersma et al. 2018). For this comparison, we consider only pixels whose geographical center is located within 50 km of the observation site, having a cloud radiance fraction < 50% and an AMF ratio ($AMF_{tropospheric}/AMF_{geometric}$) > 0.2 as recommended by Boersma et al. (2017, 2018).

Figure 9 illustrates the retrieved VCD_{tropo} for 4 days, under clear-sky conditions. We have chosen four representative days of each season of the year (May and December for the rainy season and July and August for the dry season) and in different observation geometry (zenith in 2017, 35° in 2018). The values of VCD_{tropo} are averaged (±30 min, usually around 50 measurements) around the time of the OMI overpass. Ground-based (GB) values vary between 2×10^{15} and 7×10^{15} molecules cm^{-2}, and we can observe the same type of seasonality but with differences in absolute value in particular visible on 17 August for example. The high GB values on 17 August could be associated with a high AOD value (close to 1) observed on that day (see Fig. 3). The highest NO_2 values are observed on days of the dry season while the lowest NO_2 values are observed on days of the rainy season, as illustrated in Fig. 1.

Similar to OMI, the TROPOMI is a nadir imaging spectrometer on board the *Sentinel-5* Precursor satellite, launched on 13 October 2017. It measures the sunlight reflected in the ultraviolet, visible, near-infrared, and shortwave infrared spectral ranges (Veefkind et al. 2012). With a swath width of 2600 km, it can cover the entire planet in a single day with a pixel

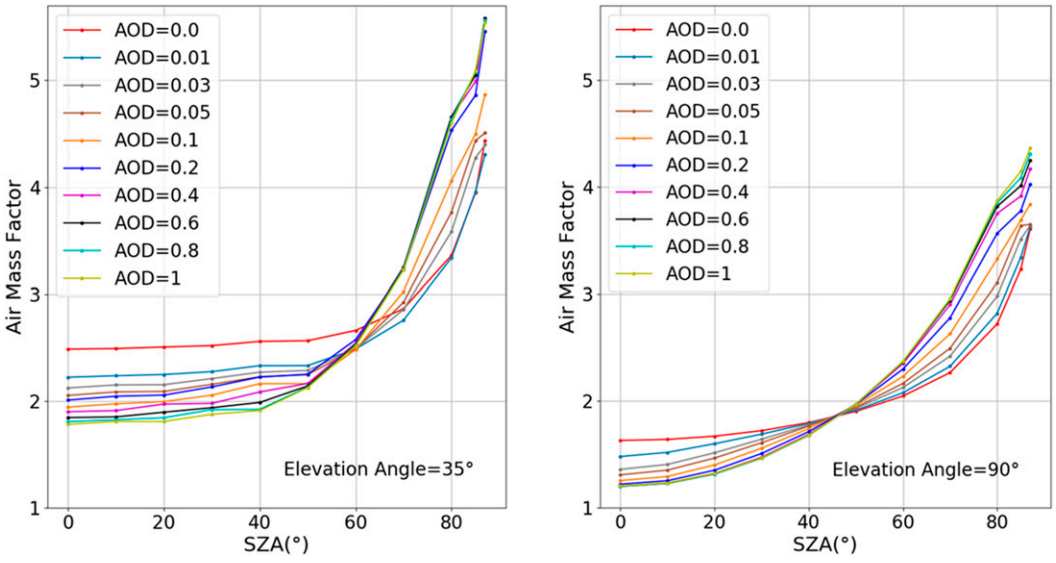

FIG. 7. Sensitivity test of tropospheric AMF with SZA and AOD variation.

size of 7 km × 3.5 km at true nadir in the UV/VIS/near-infrared bands. The spatial resolution of TROPOMI has been further improved on 6 August 2019 with a pixel size of 5.5 km × 3.5 km. Only TROPOMI ground pixels associated with a quality value ($qa_{value} > 0.75$) have been selected in our study. Following recommendations by Verhoelst et al. (2021), we used reprocessed (RPRO; v0102) and the offline (OFFL; v0102 and v0103) data products. The TROPOMI and OMI overpasses over Kinshasa occur around 1230 UTC (1330 LT). Comparisons with GB data are made using daily satellite values averaged over all selected pixels within a radius of 20 and 50 km (TROPOMI and OMI, respectively) around Kinshasa.

In Fig. 10, we show the time series of all GB measurements and satellite observations for the 2017–19 periods (see Table 1). The agreement between GB and OMI observations seems better in 2017 than in other periods of the study. This may be related to the fact that we used a different reference spectrum in the QDOAS analysis of the spectra recorded in 2018–19.

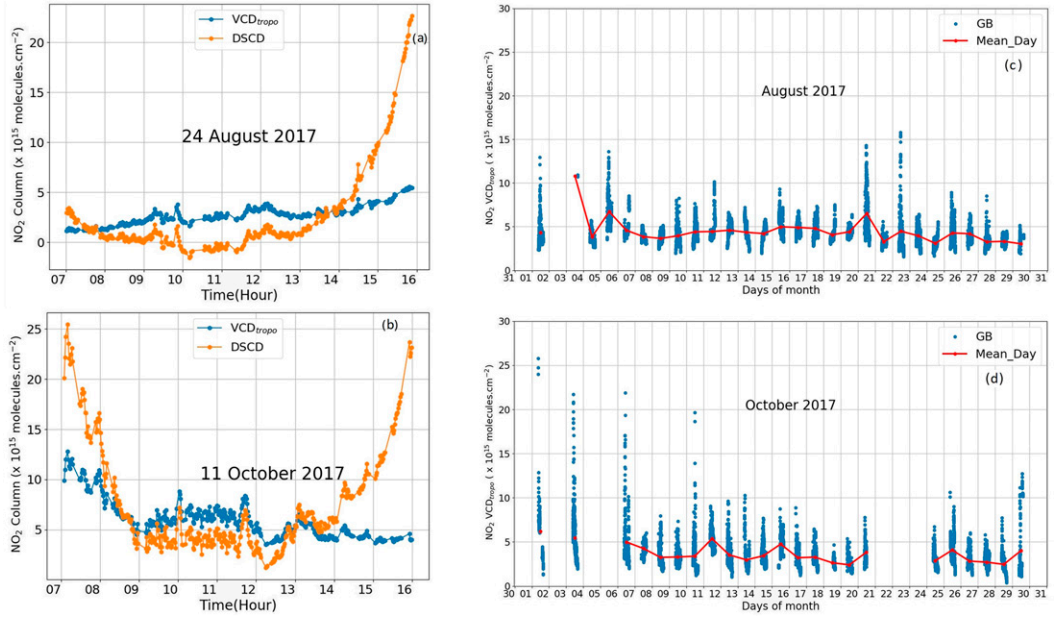

FIG. 8. Examples of ground-based DOAS measurements of NO_2 in Kinshasa. (a),(b) The VCDtropo (blue) and DSCDs (orange) for 24 Aug and 11 Oct 2017, respectively. (c),(d) The VCDtropo for Aug and Oct, respectively. The red dots in (c) and (d) show the daily averages.

TABLE 4. Error budget on recovered tropospheric NO_2 VCD. Relative (in %) and absolute errors (in molecules cm^{-2}) are given. Sigma(90) and sigma(35) indicate the two error values obtained at 90° and 35°; terms used in Eq. (6). VCD_{90} and VCD_{35} are, respectively, the propagation of these errors on the vertical column. The largest contribution comes from the error in tropospheric AMF, followed by the error in the residual column. Relative error values were found by normalizing by a typical tropospheric vertical column of 3×10^{15} molecules cm^{-2} (mean value of tropospheric VCD as measured in Kinshasa).

Error source	Sigma(90), sigma(35)	$VCD_{90°}$	$VCD_{35°}$
DSCD	0.8, 0.5 ($\times 10^{15}$)	11% (0.39)	6% (0.20)
$SCD_{residual}$	1.3, 1.8 ($\times 10^{15}$)	18% (0.63)	21% (0.75)
SCD_{strato}	0.5, 0.5 ($\times 10^{15}$)	5% (0.2)	5% (0.2)
AMF_{tropo}	0.3, 0.1	12% (0.42)	3% (0.13)
VCD	—	25% (0.89)	23% (0.81)

This second reference spectrum adds a bias of approximately 1×10^{15} molecules cm^{-2} in the calculation of VCDtropo. But it should be noted that all the GB measurements (black points) are included here, before selecting the coincident points with the satellite observations, and before flux filtering. Another point that may explain the difference in agreement between the two periods is the change in measurement geometry, from the zenith to measurements at 35° elevation in the direction of the city. The satellite measurements are always averaged within a circle of 50 or 20 km radius. So the satellite measurements are more representative of the sensitivity of the zenith measurements than the off-axis sensitivity toward the city.

Figures 11 and 12 summarize the results of our comparisons. The top panels show the linear regressions for the two cases. These are characterized by a correlation coefficient R of 0.50 and 0.72 and linear regression slopes of 0.34 and 0.41 for the OMI and TROPOMI datasets, respectively. Absolute differences (SAT-GB in $\times 10^{15}$ molecules cm^{-2}) and relative differences [(SAT − GB)/GB, in percent] were calculated for each case. For both datasets, the median bias is approximately -1.7×10^{15} molecules cm^{-2} (−46%). We calculated the bias error as the quadratic sum of GB and SAT errors plotted in Figs. 11c and 12c. For the comparison between OMI-GB and TROPOMI-GB, the mean values of these errors are 1.8×10^{15} and 0.9×10^{15} molecules cm^{-2}, respectively. The number of coincidence points for the two cases is slightly different, 51 for OMI and 44 for TROPOMI. The comparison results are obtained by removing the tropospheric VCD values of low-flux signal spectra (fluxes at 425 nm < 120 000 for the 2017 period and fluxes at 425 nm < 30 000 for 2018–19). The change in the flux filtering threshold is related to the fact that the observations made in 2018–19 were strongly influenced by dust compared to those made in 2017 and because of the change in the elevation angle in 2018. We also note that the current GB result does not change significantly when using AMFs calculated with a box profile discussed in section 3c. The test shows a median bias on the order

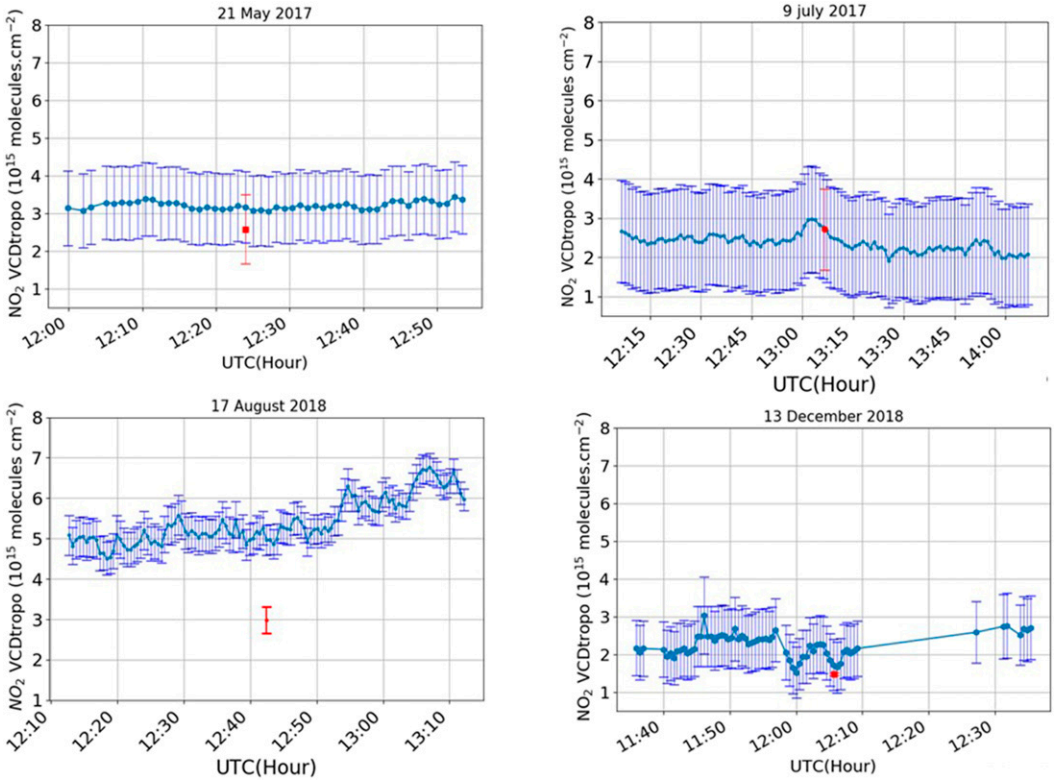

FIG. 9. Comparison of tropospheric NO_2 VCDs (blue) obtained from DSCDs measured at Kinshasa with OMI observations (red) and the corresponding error bars.

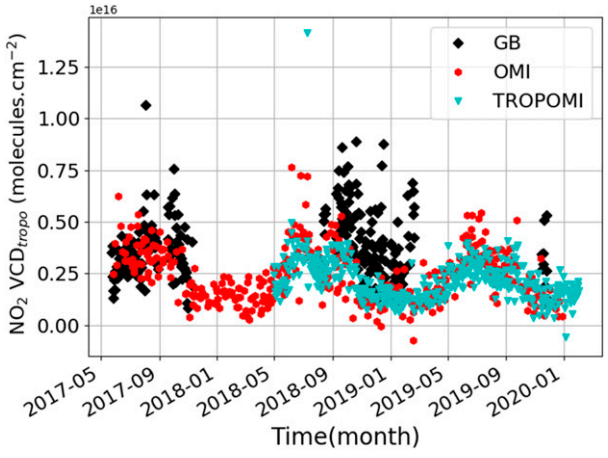

FIG. 10. A comparison of the daily average of the tropospheric vertical column of NO_2 measured in Kinshasa (black dots) against OMI (red dots) and TROPOMI (blue dots) satellite observations between 2017 and 2019. Kinshasa measurements are averaged (±30 min) around the OMI satellite overpass.

of -1.8×10^{15} molecules cm^{-2}, giving us good confidence in our GB VCDtropo retrievals.

Note that there is fewer coincidence points during the dry season. This is linked to the high aerosol load in the dry season, which leads to low ratios of AMFtropospheric/AMFgeometric, the lowest ratios being filtered out as described above. In the dry season, aerosols partly screen the surface. This strengthens the value of ground-based measurements in this area.

d. Discussion

In this subsection, we discuss the reasons for the bias observed between OMI and TROPOMI data with respect to GB. The comparisons show negative biases of approximately −46% between the two satellite instruments and GB. This negative bias may be related to the low sensitivity of satellite instruments near-surface. The typical averaging kernels as illustrated by Eskes and Boersma (2003) show that there is very little sensitivity below about 1 km, and thus the satellite retrieval strongly rely on the selected a priori profile.

For comparisons with OMI observations, a similar negative bias has been reported in urban areas (Pinardi et al. 2020) and more specifically for the African cities of Bujumbura and Nairobi (Gielen et al. 2017; Compernolle et al. 2020). This negative bias can be explained by several factors, such as the low sensitivity of satellite instruments near the surface as mentioned above, the lack of knowledge of the NO_2 a priori profile used in the AMF calculation, the coarse spatial resolution of OMI, and the systematic uncertainties in the stratospheric column estimation.

Several studies have analyzed the impact of algorithmic differences on the uncertainty of the NO_2 column, which can be as high as 42%, mainly because of the uncertainties in the AMFs due to different parameters such as surface albedo, a priori profile, and cloud parameters (Lorente et al. 2017).

Pinardi et al. (2020) showed that the relatively coarse spatial resolution of OMI (13 km × 24 km at best) affect the comparisons due to the smoothing of localized urban sources. The OMI pixels can be large compared to the size of the ground-based observation zone, including areas surrounding the observation site. The horizontal variability of NO_2 within the chosen radius of 50 km should also be considered. This may also contribute to the apparent bias found in our results. Variability of about $\pm 1 \times 10^{15}$ molecules cm^{-2} are found between the pixels in the selected radius.

Systematic uncertainties in the estimation of the stratospheric column could also contribute to this observed underestimation, given the set of small NO_2 tropospheric signals observed in African cities studied by Pinardi et al. (2020). In Kinshasa and its surroundings, values of the stratospheric vertical column approached 1.7×10^{15} molecules cm^{-2} on average compared to an average value of 3.7×10^{15} molecules cm^{-2} of the total NO_2 column. The stratospheric column of the satellite being on the same order as the tropospheric column, this may well lead to larger uncertainties in the recovery of the tropospheric column.

For comparisons with TROPOMI observations, we do not have many points of coincidence with the ground data (about 50 points, most of them in 2018). Although the GB measurements of 2019 were filtered out because of dust accumulation on the instrument's observation window, the results indicate a relatively fair level of agreement ($R = 0.72$ and slope = 0.41). Verhoelst et al. (2021) conducted a study based on the comparison of TROPOMI with the results of about 20 MAX-DOAS ground observation sites. The results of these comparisons show a negative bias of −23% to −37% in average under clean to moderate polluted conditions and large negative biases reaching about −51% in heavily polluted areas (ground-based tropospheric columns larger than 15×10^{15} molecules cm^{-2}). In our case, the results of comparisons between TROPOMI and GB for Kinshasa indicate a negative bias of −46%, thus approaching the threshold of highly polluted areas found by Verhoelst et al. (2021).

The apparent disagreements observed between TROPOMI and ground networks have been discussed in detail by Verhoelst et al. (2021). These disagreements result from errors in the retrieval of S5p tropospheric columns due to uncertainties in the a priori profile in the TM5-MP chemical transport model (horizontally coarse, 1° × 1°). Ialongo et al. (2020) and Zhao et al. (2020) showed that by using high-resolution profiles based on the regional forecast model instead of the a priori coarse NO_2 profiles used in the TM5 model, an improvement in agreement between TROPOMI and ground data was achieved. Another factor is the treatment of clouds (see Verhoelst et al. 2021). The presence of clouds and dust most of the year in Kinshasa greatly influences the observations, and the comparisons we present could be further improved by applying more advanced cloud filtering techniques, as described in Gielen et al. (2014).

Another way to improve the comparisons would be using measured NO_2 profiles from Kinshasa. Dimitropoulou et al. (2020) show in their study on TROPOMI validation with MAX-DOAS data that the use of a vertical NO_2 profile derived from ground measurements at the observation site significantly reduces the systematic underestimation of TROPOMI data. In November 2019, we have installed a new MAX-DOAS instrument on the roof of the Faculty of Science at UniKin, that will

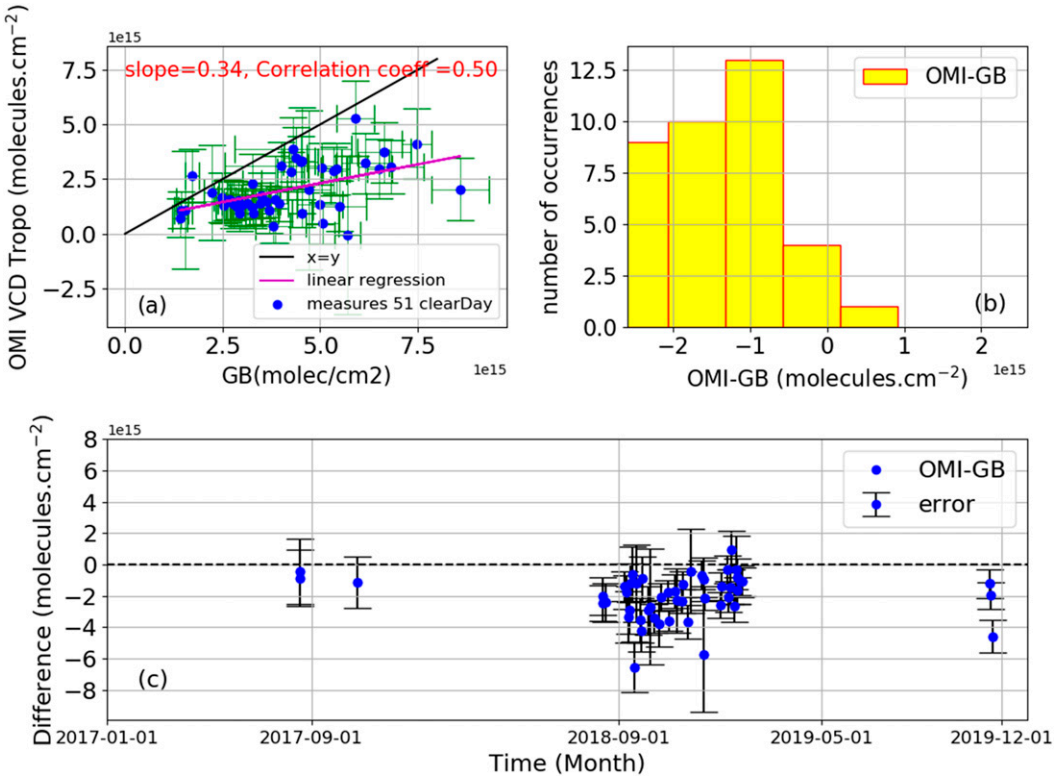

FIG. 11. (a) Linear regression analysis chart between the NO_2 tropospheric vertical columns retrieved (±30 min) around OMI observations for 51 clear days of observations. (b) Histogram of the bias between OMI and GB. (c) Time series of difference between SAT and GB. The green bars in (a) represent the uncertainty of GB and OMI, and the black error bars in (c) represent the combined error on the differences between GB and OMI in molecules cm^{-2}.

allow us to monitor the NO_2 profile in Kinshasa, offering perspectives for improving the comparison in the near future.

5. Conclusions

This work aims to present the new atmospheric observation site in Kinshasa. The city, located in the center of the African continent, is characterized by an explosive demography and a strong presence of various sources of atmospheric pollutants. In Kinshasa and its surroundings, agricultural activities leading to forest fires, biomass fires, and embers used for cooking are among the sources of air pollution. Very little research on air pollution and ground-based observations exist, although this is of great importance for the understanding of the atmosphere above this site and for the improvement of the accuracy of satellites and models. Since May 2017, we have installed a low-cost optical remote sensing instrument above the Faculty of Sciences of the University of Kinshasa. The measurements made with this instrument, which has been operating for 2 years, have allowed us to start a preliminary study of the Kinshasa atmosphere, also allowing a comparison with two satellite instruments (OMI and TROPOMI).

We measured in the zenith direction from May to November 2017. The security situation forced a change in the location of the instrument, which offered the possibility to take measurements only at an elevation angle of 35° from June 2018 to November 2019. The instability of the electricity at the observation site did not allow us to take measurements every day. Dust was also one of the problems we encountered during the observation period. Especially during the dry season, we observed the deposition of dust layers on the instrument's observation window. This dust problem makes the data unusable at times, as was the case for several days of 2019.

Using the QDOAS software, we analyzed the recorded spectra and constituted a database of DSCDs of NO_2 and trace gases. In this work, we focused on tropospheric NO_2 column retrieval. Such measurements were performed for the first time in the city of Kinshasa used them to validate tropospheric NO_2 measurements by OMI and TROPOMI satellite instruments. The mean value of VCDtropo observed in Kinshasa is 3×10^{15} molecules cm^{-2}. Comparisons with OMI observations over 51 clear days give a slope of 0.34 and a correlation coefficient of 0.50. The systematic bias between OMI and ground-based data can be related to the unknown NO_2 profile in Kinshasa and also to the coarse horizontal resolution of the OMI instrument. With only 44 days coincident between GB and TROPOMI, we observe a slope of 0.41 and a correlation coefficient of 0.72. The correlation is better with TROPOMI, which can be understood by the better resolution of TROPOMI and thus spatial matching between ground-based and spaceborne measurements. The negative bias is a robust finding of the study as it is observed in both OMI and TROPOMI. Although this is a common feature in other satellite

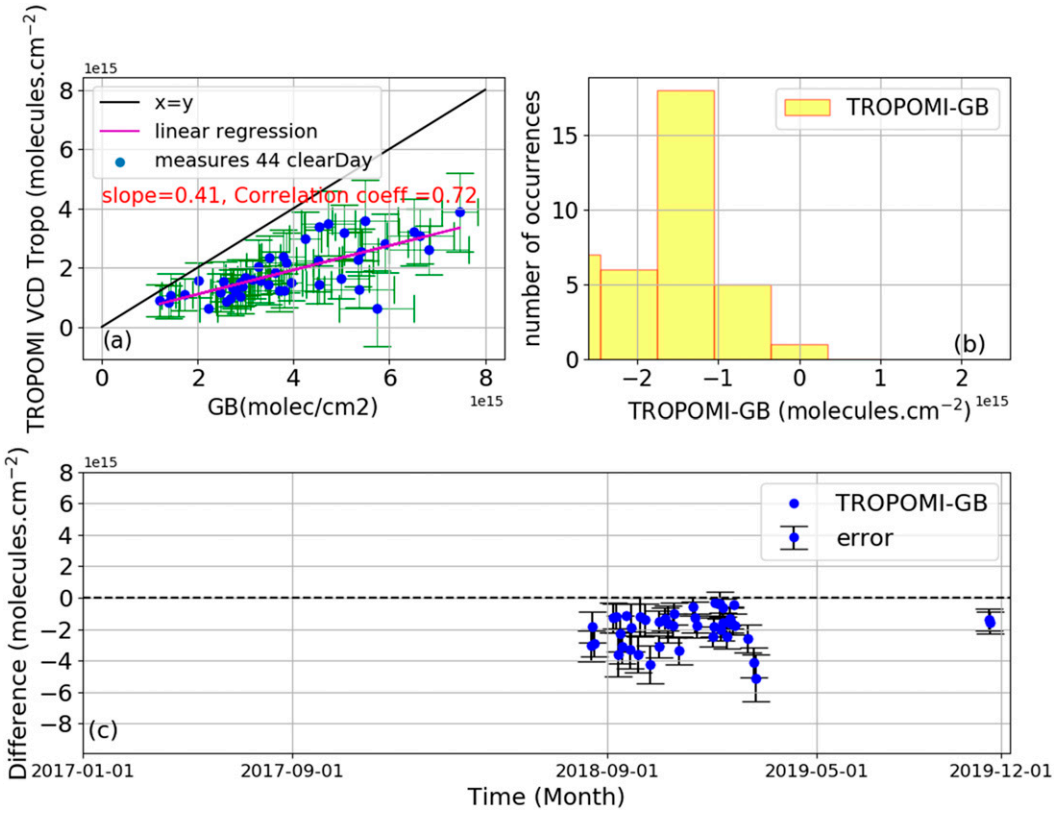

FIG. 12. (a) Linear regression analysis chart between the NO_2 tropospheric vertical columns retrieved (±30 min) around TROPOMI observations for 44 clear days of observations. (b) Histogram of the bias between TROPOMI and GB. (c) Time series of difference between SAT and GB. The green bars in (a) represent the uncertainty of GB and TROPOMI, and the black error bars in (c) represent the combined error on the differences between GB and TROPOMI in molecules cm^{-2}.

versus GB measurement comparisons, this motivates further investigations. These comparisons are preliminary. Indeed, more data will be needed to confirm our first comparisons while we foresee that in-depth data filtering dealing with a larger number of coincidences and GB profile data availability will help to improve the comparisons with satellite measurements.

At the time of closing this paper, it is worth noting that a MAX-DOAS instrument has been installed in Kinshasa since November 2019. This opens interesting prospects for the near future, since this instrument can provide very useful information such as the profiles of the main absorbers (NO_2 and H_2CO). This will strengthen forthcoming studies addressing the precise assessment of air quality in Kinshasa and central Africa, making use of an improved DOAS instrument and exploiting a chemistry transport model.

Acknowledgments. We thank the Belgian Federal Science Policy Office (BELSPO) and the KinAERO Project for their financial support. Rodriguez Yombo Phaka benefits from a scholarship funded by the Académie de Recherche et d'Enseignement Supérieur–Commission de la Coopération au Développement (ARES–CCD), managed at ULiège by the Centre pour le Partenariat et la Coopération au Développement (PACODEL). Emmanuel Mahieu is a senior research associate with the F.R.S.–FNRS. We thank Claudio Queirolo for his valuable contribution in the realization of the few materials used in this work. We thank Robert Spurr for free deployment of VLIDORT. The MERRA-2 data used in this study have been provided by the Global Modeling and Assimilation Office (GMAO) at NASA Goddard Space Flight Center. We also thank Nuno Pereira for useful discussions and the late Professor Jacob Sabkinu for his support of our project.

Data availability statement. The spectra, DSCDs, and VCD supporting the conclusions of this study are available from BIRA-IASB. The GEOS-Chem data are available from ULiège. All these data are available upon request. Please contact the authors.

REFERENCES

Bey, I., and Coauthors, 2001: Global modeling of tropospheric chemistry with assimilated meteorology: Model description and evaluation. *J. Geophys. Res.*, **106**, 23 073–23 095, https://doi.org/10.1029/2001JD000807.

Boersma, K. F., and Coauthors, 2017: QA4ECV product specification document for the QA4ECV NO_2 ECV Precursor product. *Atmos. Meas. Tech.*, **11**, 1–32.

——, and Coauthors, 2018: Improving algorithms and uncertainty estimates for satellite NO_2 retrievals: Results from the quality

assurance for the essential climate variables (QA4ECV) project. *Atmos. Meas. Tech.*, **11**, 6651–6678, https://doi.org/10.5194/amt-11-6651-2018.

Bogumil, K., and Coauthors, 2003: Measurements of molecular absorption spectra with the SCIAMACHY pre-flight model: Instrument characterization and reference data for atmospheric remote-sensing in the 230–2380 nm region. *J. Photochem. Photobiol.*, **157A**, 167–184, https://doi.org/10.1016/S1010-6030(03)00062-5.

Brewer, A. W., C. T. McElroy, and J. Kerr, 1973: Nitrogen dioxide concentration in the atmosphere. *Nature*, **246**, 129–133, https://doi.org/10.1038/246129a0.

C3S, 2017: ERA5: Fifth generation of ECMWF atmospheric reanalyses of the global climate. Copernicus Climate Change Service CDS, accessed 24 September 2019, https://cds.climate.copernicus.eu/cdsapp#!/home.

Chan, A. W., and Coauthors, 2010: Role of aldehyde chemistry and NO_x concentrations in secondary organic aerosol formation. *Atmos. Chem. Phys.*, **10**, 7169–7188, https://doi.org/10.5194/acp-10-7169-2010.

Chance, K. V., and R. J. D. Spurr, 1997: Ring effect studies: Rayleigh scattering, including molecular parameters for rotational Raman scattering, and the Fraunhofer spectrum. *Appl. Opt.*, **36**, 5224–5230, https://doi.org/10.1364/AO.36.005224.

——, and R. L. Kurucz, 2010: An improved high-resolution solar reference spectrum for Earth's atmosphere measurements in the ultraviolet, visible, and near infrared. *J. Quant. Spectrosc. Radiat. Transfer*, **111**, 1289–1295, https://doi.org/10.1016/j.jqsrt.2010.01.036.

Chen, D., B. Zhou, S. Beirle, L. M. Chen, and T. Wagner, 2009: Tropospheric NO_2 column densities deduced from zenith-sky DOAS measurements in Shanghai, China, and their application to satellite validation *Atmos. Chem. Phys.*, **9**, 3641–3662, https://doi.org/10.5194/acp-9-3641-2009.

Compernolle, S., and Coauthors, 2020: Validation of Aura-OMI QA4ECV NO_2 climate data records with ground-based DOAS networks: The role of measurement and comparison uncertainties *Atmos. Chem. Phys.*, **20**, 8017–8045, https://doi.org/10.5194/acp-20-8017-2020.

Constantin, D. E., A. Merlaud, M. V. Roozendael, M. Voiculescu, C. Fayt, F. Hendrick, G. Pinardi, and L. Georgescu, 2013: Measurements of tropospheric NO_2. *Sensors*, **13**, 3922–3940, https://doi.org/10.3390/s130303922.

Crutzen, P. J., 1979: The role of NO and NO_2 in the chemistry of the troposphere and stratosphere *Annu. Rev. Earth Planet. Sci.*, **7**, 443–472, https://doi.org/10.1146/annurev.ea.07.050179.002303.

Danckaert, T., C. Fayt, M. Van Roozendael, I. De Smedt, V. Letocart, A. Merlaud, and G. Pinardi, 2017: QDOAS software user manual. Royal Belgian Institute for Space Aeronomy (BIRA) Doc., 71 pp.

Dimitropoulou, E., and Coauthors, 2020: Validation of TROPOMI tropospheric NO_2 columns using dual-scan multi-axis differential optical absorption spectroscopy (MAX-DOAS) measurements in Uccle, Brussels. *Atmos. Meas. Tech.*, **13**, 5165–5191, https://doi.org/10.5194/amt-13-5165-2020.

Errera, Q., and D. Fonteyn, 2001: Four-dimensional variational chemical assimilation of CRISTA stratospheric measurements. *J Geophys. Res.*, **106**, 12 253–12 265, https://doi.org/10.1029/2001JD900010.

Eskes, H. J., and K. F. Boersma, 2003: Averaging kernels for DOAS total-column satellite retrievals. *Atmos. Chem. Phys.*, **3**, 1285–1291, https://doi.org/10.5194/acp-3-1285-2003.

Friedrich, M., C. Rivera, W. Stremme, Z. Ojeda, J. Arellano, A. Bezanilla, J. A. García-Reynoso, and M. Grutter, 2019: NO_2 vertical profiles and column densities from MAX-DOAS measurements in Mexico City. *Atmos. Meas. Tech.*, **12**, 2545–2565, https://doi.org/10.5194/amt-12-2545-2019.

Gielen, C., and Coauthors, 2014: A simple and versatile cloud-screening method for MAX-DOAS retrievals. *Atmos. Meas. Tech.*, **7**, 3509–3527, https://doi.org/10.5194/amt-7-3509-2014.

——, and Coauthors, 2017: Characterisation of central-African aerosol and trace-gas emissions based on MAX-DOAS measurements and model simulations over Bujumbura, Burundi. *Atmos. Chem. Phys. Discuss.*, https://doi.org/10.5194/acp-2016-1104.

Harder, J. W., and J. W. Brault, 1997: Atmospheric measurements of water vapor in the 442-nm region. *J. Geophys. Res.*, **102**, 6245–6252, https://doi.org/10.1029/96jd01730.

Hendrick, F., and Coauthors, 2004: Retrieval of nitrogen dioxide stratospheric profiles from ground-based zenith-sky UV-visible observations: Validation of the technique through correlative comparisons. *Atmos. Chem. Phys.*, **4**, 2867–2904, https://doi.org/10.5194/acpd-4-2867-2004.

Hermans, C., and Coauthors, 2003: Absorption cross-section of the collision-induced bands of oxygen from the UV to the NIR. *Weakly Interacting Molecular Pairs: Unconventional Absorbers of Radiation in the Atmosphere*, C. Camy-Peyret and A. A. Vigasin, Eds., NATO Science Series IV, Vol. 27, Springer, 193–202.

Hönninger, G., C. von Friedeburg, and U. Platt, 2004: Multi axis differential optical absorption spectroscopy (MAX-DOAS). *Atmos. Chem. Phys.*, **4**, 231–254, https://doi.org/10.5194/acp-4-231-2004.

Ialongo, I., H. Virta, H. Eskes, J. Hovila, and J. Douros, 2020: Comparison of TROPOMI/Sentinel-5 Precursor NO_2 observations with ground-based measurements in Helsinki. *Atmos. Meas. Tech.*, **13**, 205–218, https://doi.org/10.5194/amt-13-205-2020.

Katoto, P. D., and Coauthors, 2019: Ambient air pollution and health in sub-Saharan Africa: Current evidence, perspectives and a call to action. *Environ. Res.*, **173**, 174–188, https://doi.org/10.1016/j.envres.2019.03.029.

Knippertz, P., M. J. Evans, P. R. Field, A. H. Fink, C. Liousse, and J. H. Marsham, 2015: The possible role of local air pollution in climate change in West Africa. *Nat. Climate Change*, **5**, 815–822, https://doi.org/10.1038/nclimate2727.

Kramer, L. J., R. J. Leigh, J. J. Remedios, and P. S. Monks, 2008: Comparison of OMI and ground-based in situ and MAX-DOAS measurements of tropospheric nitrogen dioxide in an urban area. *J. Geophys. Res.*, **113**, D16S39, https://doi.org/10.1029/2007JD009168.

Levelt, P. F., and Coauthors, 2006: The Ozone Monitoring Instrument. *IEEE Trans. Geosci. Remote Sens.*, **44**, 1093–1101, https://doi.org/10.1109/TGRS.2006.872333.

Liousse, C., E. Assamoi, P. Criqui, C. Granier, and R. Rosset, 2014: Explosive growth in African combustion emissions from 2005 to 2030. *Environ. Res. Lett.*, **9**, 035003, https://doi.org/10.1088/1748-9326/9/3/035003.

Lorente, A., and Coauthors, 2017: Structural uncertainty in air mass factor calculation for NO_2 and HCHO satellite retrievals. *Atmos. Meas. Tech.*, **10**, 759–782, https://doi.org/10.5194/amt-10-759-2017.

Mayer, B., and A. Kylling, 2005: The libRadtran software package for radiative transfer calculations—Description and examples of use. *Atmos. Chem. Phys.*, **5**, 1855–1877, https://doi.org/10.5194/acp-5-1855-2005.

Molina, M. J., and L. T. Molina, 2004: Megacities and atmospheric pollution. *J. Air Waste Manage. Assoc.*, **54**, 644–680, https://doi.org/10.1080/10473289.2004.10470936.

Noxon, J. F., 1975: Nitrogen dioxide in the stratosphere and troposphere measured by ground-based absorption spectroscopy. *Science*, **189**, 547–549, https://doi.org/10.1126/science.189.4202.547.

Pinardi, G., and Coauthors, 2020: Validation of tropospheric NO_2 column measurements of GOME-2A and OMI using MAX-DOAS and direct sun network observations. *Atmos. Meas. Tech.*, **13**, 6141–6174, https://doi.org/10.5194/amt-13-6141-2020.

Platt, U., and J. Stutz, 2008: *Differential Optical Absorption Spectroscopy*. Springer, 608 pp., https://doi.org/10.1017/CBO9781107415324.004.

Roy, R., 2016: The cost of air pollution in Africa. OECD Development Centre Working Paper. Tech. Rep. 333, 56 pp.

Saint-Moulin, L., 2011: Atlas de l'organisation administrative de la République démocratique du Congo. 2nd ed. Centre d'études pour l'action sociale Doc., 234 pp., http://mukanda.univ-lorraine.fr/biblio/atlas-de-lorganisation-administrative-de-la-republique-democratique-du-congo-2e-edition-revue.

Shomba Kinyamba, S., F. Mukoka Nsenda, D. Olela Nonga, T. Kaminar, and W. Mbalanda, 2015: *Monographie de la ville de Kinshasa*. Centre de recherches pour le développement international, 105 pp.

Solomon, S., R. W. Portmann, R. W. Sanders, J. S. Daniel, W. Madsen, B. Bartram, and H. Cavendish, 1999: On the role of nitrogen dioxide in the absorption of solar radiation. *J. Geophys. Res.*, **104**, 12 047–12 058, https://doi.org/10.1029/1999JD900035.

Spurr, R., 2013: User's guide: VLIDORT—Version 2.6. RT Solutions Doc., 122 pp.

Tack, F., and Coauthors, 2015: Tropospheric nitrogen dioxide column retrieval from ground-based zenith-sky DOAS observations. *Atmos. Meas. Tech.*, **8**, 2417–2435, https://doi.org/10.5194/amt-8-2417-2015.

UN, 2016: The world's cities in 2016. UN Dept. of Economic and Social Affairs Data Booklet, 29 pp.

Vandaele, A. C., and Coauthors, 1998: Measurements of the NO_2 absorption cross-section from 42 000 cm^{-1} to 10 000 cm^{-1} (238–1000 nm) at 220 K and 294 K. *J. Quant. Spectrosc. Radiat. Transfer*, **59**, 171–184, https://doi.org/10.1016/S0022-4073(97)00168-4.

Van Roozendael, M., and F. Hendrick, 2012: Recommendations for NO2 column retrieval from NDACC zenith-sky UV-VIS spectrometers. Belgian Institute for Space Aeronomy (BIRA-IASB) Tech. Rep. 2, 7 pp.

Veefkind, J. P., and Coauthors, 2012: TROPOMI on the ESA Sentinel-5 Precursor: A GMES mission for global observations of the atmospheric composition for climate, air quality and ozone layer applications. *Remote Sens. Environ.*, **120**, 70–83, https://doi.org/10.1016/j.rse.2011.09.027.

Verhoelst, T., and Coauthors, 2021: Ground-based validation of the Copernicus Sentinel-5p TROPOMI NO_2 measurements with the NDACC ZSL-DOAS, MAX-DOAS and Pandonia global networks. *Atmos. Meas. Tech.*, **14**, 481–510, https://doi.org/10.5194/amt-14-481-2021.

WHO, 2006: Air quality guidelines for Europe. WHO Tech. Rep., 288 pp.

Yombo, R., G. Pinardi, A. Merlaud, C. Fayt, M. Van Rozendael, and P. Mbungu, 2018: DOAS measurements from Kinshasa: Context and first results. *20th EGU General Assembly*, Vienna, Austria, EGU2018-6924.

Zhao, X., and Coauthors, 2020: Assessment of the quality of TROPOMI high-spatial-resolution NO_2 data products in the greater Toronto area. *Atmos. Meas. Tech.*, **13**, 2131–2159, https://doi.org/10.5194/amt-13-2131-2020.